minerals

MDPI

Article

A New Approach to Predicting Vertical Permeability for Carbonate Rocks in the Southern Mesopotamian Basin

Emad A. Al-Khdheeawi [1,2,*], Raed H. Allawi [3,4], Wisam I. Al-Rubaye [5] and Stefan Iglauer [6]

1 Oil and Gas Engineering Department, University of Technology-Iraq, Baghdad 10066, Iraq
2 Western Australian School of Mines: Minerals, Energy and Chemical Engineering, Curtin University, Perth, WA 6102, Australia
3 Petroleum Engineering College, Al-Ayen University, Nasiriyah 64001, Iraq
4 Thi-Qar Oil Company, Nasiriyah 64001, Iraq
5 Ministry of Oil, Baghdad 00964, Iraq
6 School of Engineering, Edith Cowan University, Perth, WA 6027, Australia
* Correspondence: emad.al-khdheeawi@curtin.edu.au or 150070@uotechnology.edu.iq

Abstract: Reservoir performance depends on many factors, and the most important one is permeability anisotropy. In addition, with high heterogeneity, it is essential to find unique relationships to predict permeability. Therefore, this study aims to predict vertical permeability based on horizontal permeability and porosity and to find new equations for carbonate reservoirs. This work relied on the 398 measured points of cores data collected from several wells in carbonate reservoirs. A new correlation for predicting vertical permeability for the whole data (369 samples) as a function of horizontal permeability and porosity has been developed. The results indicate that this new correlation can estimate the vertical permeability with correlation coefficients (RSQ) of 0.853. Then, the used data were divided into four groups depending on the Kv/Kh values: less than 0.1, 1–0.1, 1–10, and more than 10, and a new correlation for permeability prediction for each group has been developed with good RSQ values of 0.751, 0.947, 0.963, and 0.826, respectively. The previous studies lack the correlations to predict vertical permeability in carbonate reservoirs, so this study can be considered as a reference for similar cases.

Keywords: vertical permeability; horizonal permeability; carbonate rocks; heterogeneity; correlation

check for updates

Citation: Al-Khdheeawi, E.A.; Allawi, R.H.; Al-Rubaye, W.I.; Iglauer, S. A New Approach to Predicting Vertical Permeability for Carbonate Rocks in the Southern Mesopotamian Basin. *Minerals* **2023**, *13*, 1519. https://doi.org/10.3390/min13121519

Academic Editors: Yi Fang, Brandon Schwartz, Yong Li and Zhuang Sun

Received: 2 September 2023
Revised: 30 November 2023
Accepted: 2 December 2023
Published: 4 December 2023

1. Introduction

Permeability is a crucial factor in the characterization of oil and gas reservoirs as it regulates how fluids flow through it [1]. The complexity of formation continuity and, particularly, the differences in pore space-related parameters like porosity, permeability, and capillary pressure are becoming increasingly apparent to the oil industry. Among all the formation parameters that oil and gas engineers use, permeability is one of the most crucial. It is used to decide whether to complete and put a well into operation or to leave it abandoned. The initial depositional process as well as later diagenetic and tectonic modifications are reflected in these variances. For the purpose of forecasting the performance of reservoirs and creating a management plan for field production, simple models frequently fall short. Reservoir engineers are realizing more and more how critical it is to optimize recovery based on the reservoir properties. As a result, a precise understanding of the distribution of permeability both vertically and laterally is crucial.

Because it regulates production rate, permeability is a crucial factor in reservoir development and management. In general, increased porosity, larger grains, and better sorting all result in an increase in permeability. Permeability has been studied extensively in carbonate formations for many years. It has long been thought that vertical permeability in carbonate formations is problematic. In carbonates, pore connectivity is the primary factor influencing permeability [2]. Carbonate reservoirs exhibit heterogeneity as a result of different depositional conditions and subsequent diagenetic processes. Most heterogeneous reservoirs are composed of formations that have varying pore geometry and/or contain shale. Reservoir heterogeneity is now seen as an opportunity to recover more oil rather than a concern in this instance. The reservoirs are considered to be nonuniform, isotropic, and homogeneous in early reservoir engineering research. But in more recent research, a more accurate representation of the reservoir's complicated geological consistency has been obtained through the application of permeability–porosity relationships.

The deposited environment has a crucial role in the formation of primary porosity [3]. Porosity and permeability are typically higher in high-energy deposits than low-energy deposits, which have lower permeable intervals. Low-energy deposits frequently have high porosity; however, permeability may also be low if the pore throat size is too tiny. Porosity is both created by and destroyed by diagenesis [4]. For instance, early cementation may prevent compaction and retain primary porosity by reducing porosity and permeability, whereas dissolution primarily enhances porosity with the exception of specific stylolites that may form barriers. Because it is difficult to assess directly, permeability prediction presents a challenge for information appraisal and reservoir modeling. Understanding permeability is crucial for creating 3D reservoir models, comprehending oil and gas production, and, ultimately, developing a development strategy [5].

Traditional methods of determining permeability include core analysis and well testing. These traditional techniques are very time and money consuming. The difficulty of precisely estimating permeability in diverse carbonate reservoirs is challenging [6]. Several studies attempted to use intricate mathematical formulae to relate permeability and reservoir characteristics; nevertheless, this led to an inaccurate calculation of the formation permeability values. The most popular technique for figuring out permeability is called conventional core analysis, which forms a nonlinear relationship between porosity and permeability [7]. By using this connection, permeability as a function of porosity can be predicted. Vertical permeability is one of the most important reservoir characteristics due to its great role in various oil field activities such as optimizing the well location, production rate, directional drilling, completion method, and perforation properties. Permeability anisotropy, the ratio of vertical to horizontal permeability, is vital in reservoir modeling due to its role in both vertical and horizontal wells.

In multilayered reservoirs, each layer has distinct vertical permeability [8]. Thus, these are reservoirs usually classified based on their permeability anisotropy (the ratio of vertical permeability (Kv) to horizontal permeability (Kh)). In earlier reservoir engineering research, reservoirs were proposed to be nonuniform but isotropic and homogeneous. However, recent studies describe the reservoir as heterogeneous in terms of permeability and porosity [9,10]. Generally, the horizontal permeability is higher than the vertical permeability for rocks with nonuniform and large grains [11–14], which is the case in most hydrocarbon reservoirs. Clark [14] also demonstrated that the permeability of the rock would be very high and nearly identical in both vertical and horizontal directions if it were primarily made up of large, uniformly rounded grains. Generally speaking, horizontal permeability is greater than vertical permeability, especially when the sand grains are tiny and irregularly shaped. This group includes a large proportion of the oil and gas reservoirs.

Various studies have been performed to estimate the absolute permeability of different carbonate and sandstone reservoirs [15–19]. It is important to mention that predicting permeability and developing a straight equation for permeability as a function of petrophysical properties for carbonate reservoirs is a complicated task because of the availability of several uncertainties (e.g., anisotropy and heterogeneity) in these reservoirs. Thus, many researchers used core analysis measurements to predict permeability [20–22]. Therefore, rock permeability is impacted by several factors, including the form, size, and shape of the grains that constitute the reservoir formations. These factors and the permeability of the rocks are determined using laboratory tests on the core samples. Laboratory tests are usually rare and expensive. In addition, these tests do not represent the whole reservoir because the core samples are taken at specific depths and there is a lack of vertical permeability measurements.

Thus, it is crucial to develop a relationship to predict the vertical permeability based on available core measurement data. To do so, a relationship between microscopic core data and microscopic-level attributes using the concept of hydraulic mean radius should be developed. Permeability–porosity variations in this concept are characterized as ($\sqrt{K/\varnothing_e}$).

The groundbreaking equation for predicting the permeability–porosity relationship was developed by Kozeny [22]. Carman [23] modified the Kozeny equation and developed the modified Kozeny–Carman equation [24]:

$$K = \left(\frac{\varnothing_e^3}{(1-\varnothing_e)^2} \right) \times \left[\frac{1}{F_s \tau^2 S_{gr}^2} \right] \tag{1}$$

where K is permeability, $\varnothing_e$ is effective porosity, F_s is 3D pore shape factor, τ is tortuosity, and S_{gr} is specific surface area per unit volume.

Equation (1) can be rearranged in terms of the hydraulic mean radius variations ($\sqrt{K/\varnothing_e}$) by dividing both sides by effective porosity $(\varnothing_e)$ and taking the square root for both sides as follows:

$$\sqrt{\frac{K}{\varnothing_e}} = \left(\frac{\varnothing_e}{1-\varnothing_e} \right) \times \left[\frac{1}{\sqrt{F_s}\, \tau S_{gr}} \right] \tag{2}$$

In addition, to simplify the prediction of the permeability–porosity relationship, the reservoir quality index (RQI) has been proposed as a function of hydraulic mean radius variations ($\sqrt{K/\varnothing_e}$). The RQI model considers the pore, pore throat, and grain distributions with other macroscopic parameters [25]:

$$RQI\ (\mu m) = 0.0324 \left(\sqrt{\frac{K}{\varnothing_e}} \right) \tag{3}$$

Based on the RQI model, Zahaf and Tiab [26] developed a generalized equation for predicting vertical permeability (K_v) as a function of hydraulic mean radius by substituting horizontal permeability (K_h) instead of absolute permeability (K):

$$K_v = A \times \left(\sqrt{\frac{K_h}{\varnothing_e}} \right)^B \tag{4}$$

where A and B are specific field case coefficients.

However, all previous equations for predicting vertical permeability were developed for sandstone reservoirs. Even though the uncertainties in carbonate reservoirs in terms of anisotropy and heterogeneity are well known, the prediction of the vertical permeability of carbonate reservoirs has not received sufficient attention. Thus, in this paper, new sets of correlations have been developed to predict vertical permeability for carbonate reservoirs as a function of horizontal permeability and porosity using 369 laboratory measurements.

2. Stratigraphic Description and Facies Analysis

The Arabian Plate is positioned to the north of the Mesopotamian Basin. In the west and east, respectively, this foreland basin empties into the folded zone of the Arabian stable shelf's Salman zone. The rocks in the basin's basement are metamorphic Precambrian rocks. The majority of the infracambrain to quaternary rocks make up the sedimentary cover, which thickens toward the east. The extensional and compressional tectonic stages are the two distinct stages of the Cretaceous tectonic growth of the Mesopotamian Basin. A passive global border sedimentary setting was formed by the South-Neo-Tethys between the Late Tithonian and the Early Turonian. The closure created a compression tectonic stage between the Late Turonian and Maastrichtian, which led to the Arabian Plate entering the foreland basin evolution stage. Folds with basement involvement are known as anticlines, and they are found in the southern and central Mesopotamian Basins [27].

The southern Mesopotamian Basin, a transitional region between the Arabian Plate and the Zagros Mountains, is where the region of study is located. Due to various forces (e.g., climatic, eustatic, and tectonic), more than 3500 m of Cretaceous deposits have settled across this region. During the period of the Cretaceous, the region was a portion of a wider limestone layer that was situated along the Arabian Plate's northeast passive border. The Mesopotamian basin's Cretaceous succession consists of six supersequences. They are all separated from one another by maximum flooding surfaces and unconformities. Limestone dominated the studied carbonate formation, which is called the Mishrif Formation [28]. The Mishrif Formation is made up of three third-order sequences stratigraphically. Each of them is made up of an upper regressive and a lower transgressive hemicycle. Either conformity or disconformity layers separate each of the third-order sequences, and mudstone and wackestone are the predominant grains on all maximum flooding surfaces. This formation is divided into three members. These members can be further divided into six zones, six subzones, and 7–8 strata. The three primary pore types created in this formation are microfracture pores, matrix pores, and dissolved vug. The formation is split into three 3rd-order sequences. There are algal, bioclastic, rudistid, and foraminiferal-rich facies in the heterogeneous carbonates of the Mishrif Formation. They are split into two permanent restrictive cycles by the facies growth and an unconformity surface at the region level. According to current biostratigraphic research, the formation is early–late Cenomanian, but the dating system places it in the middle of the Centaurus–early Turonian period. Along the Mishrif platform, the border between Iran and Iraq exhibits a high energy trend with a thickness of about 400 m [27,28].

Seven facies, spanning from shallow open marine Tidal Flat, are recognized that correspond to palaeo-depositional environments. The paleo-geomorphy decreased toward the north when the formation as a whole was being deposited [29]. The paleo-geomorphical trend is controlling the decline in Mishrif's thickness especially around the carbonate ramp and the reef-rimmed carbonate platform. Considering the specific palaeo-geographical setting throughout this basin, rudist congregations might move lateral into shoal facies or be displaced by them, which occupied the platform margin in this depositional model without forming a continuous rim. The historic slope break on this limestone platform is its most noticeable feature. The relationships between these facies are outlined below [30,31].

2.1. Deep Marine Facies

The micritic and argillaceous limestones that make up the units of deep marine facies range in thickness from 1 to 40 m, and they are accompanied by thin shales. Limestones are made up of fine-grained bioclasts that have been carried from nearby shallow-shelf regions as well as wackestones and mudstones that are rich in pelagic foraminifera. Deposition occurred beneath the base of the storm wave as well as the photic zone. Both the photic zone and the storm wave base were below which deposition occurred.

2.2. Shallow-Shelf Open Marine

There were six identified microfacies in this facies type of Mishrif Formation. The thick and massive units of limestone that make up the faces are made up of bioclastic wackestones and packstones. Green algae, mixed rudist, bivalves, and echinoids debris, as well as benthonic and planktonic foraminifera, are examples of bioclasts. Algae and colonial corals are also found. Shallow-shelf open-marine facies become increasingly rudist- and grain-rich as they move upward. The rudist debris was carried downslope and deposited as packstones and floatstones, suggesting that it originated from adjacent rudist biostromes. This facies association contains high porosity, grain-rich bioclastic limestones.

2.3. Rudist Biostromes

Throughout rudstones and packstones, para-autochthonous and autochthonous rudists predominate in rudist biostromes. Rudist bioclasts tend to be highly compacted, usually broken but rarely rounded, and poorly arranged. Rudists in the Mishrif Formation lack characteristics of reefs or build-ups; as a result, rudist structures are called lithosomes, and dense faunal groups are called congregations.

2.4. Shoal Facies

Grain-dominated packstones and grainstones make up the majority of the shoal facies. Rudists, echinoderms, algae, pellets, and coated grains are examples of bioclasts. Small benthonic foraminifera, mollusks, and allochthonous corals are also found locally, although their poor preservation suggests lengthy transport routes.

It is believed that the shoal facies deposits contain very little clay because they were deposited above the fairweather wave base in high energy settings.

2.5. Back-Shoal Facies

This type is varying from bioclastic and foraminiferal-rich wackestones to packstones formed of shoals or rudist biostromes during comparatively calm water conditions. In addition to the less common elements such as pellets, algae, echinoderms, gastropods, and benthonic foraminifera, bioclasts consist of fragments of coarse rudist and Chondrodonta bivalve. It is believed that the back-shoal facies originated in photic environments with low energy and shallow water.

2.6. Lagoonal Facies

Lagoonal facies, which are found in specific regions of the Mishrif, are identified through a range of benthonic foraminiferal species, such as textulariids, milolids, and alveolinids. Spicules of sponge, rudist pieces, gastropods, and ostracods are found locally and exhibit minimal breakage, suggesting short transport distances. Deposits of lagoon facies can have a thickness of over 30 m.

Thin layers of grainstones and peloidal and rudistid packstones may be found within the lagoonal successions. These are believed to be small-scale biostromes and shoals that developed in the lagoonal environment.

2.7. Tidal Flat Facies

The top part the Mishrif contains tidal flat facies, which are composed of lime mudstones with poor fossil preservation and Charophyta wackestones.

Deposits on tidal flat facies are frequently highly recrystallized, oxidized, and bleached. Although facies are difficult to distinguish from lagoonal deposits, thicknesses vary from 1 to 15 m.

3. Materials and Methods

A total of 369 experimental samples from various depths of a carbonate formation were collected from an Iraqi southern oil field. For all 369 samples, the porosity, horizontal permeability, and vertical permeability were recorded as a function of depth. All the samples were loaded for Soxhlet cleaning using refluxing hot toluene and methanol. Samples are deemed clean when no further evidence of hydrocarbons (fluorescence under UV light) or salts (silver nitrate precipitation) is present. After cleaning, the samples were then dried in a regular oven at 116 °C. Once dried, the plug samples were stored in a desiccator and allowed to cool to room temperature prior to the analysis. The weight of each sample was determined. The direct grain volume of all plug samples was then determined using Core Laboratories Ultra-poreTM 400 (Core Laboratories, Houston, TX, USA). The grain density is determined by dividing the dry weight of the plug by the grain volume determined by the Ultra-poreTM 400. Ultra-poreTM 400 uses Boyles's law to determine the pore or grain volume from the expansion of a known mass of helium into a calibrated sample holder.

The equation used for the calculation of grain volume is derived from the basic Boyle's law as follows:

$$P_1V_1 = P_2V_2 \tag{5}$$

which can be expressed in term of grain volume:

$$V_g = (V_r + V_m) - \frac{P_1}{P_2} V_r \tag{6}$$

where V_g is the grain volume of the sample, V_m is the matrix cup volume (sample holder), V_r is the known reference volume (filled by helium), P_1 is the initial pressure, and P_2 is the expanded pressure.

The bulk volume (V_b) is calculated by measuring the dimensions of the sample. Then, pore volume (V_p) and porosity (ø) are calculated as follows:

$$V_p = V_b - V_g \tag{7}$$

$$ø = \frac{V_p}{V_b} \tag{8}$$

Pore volume measurements were made using the Boyles law method combined with an advanced calibration technique. The effective porosity of each sample was then calculated using the pore volume determined at the designated confining stresses by the CMSTM—300 and the direct grain volume from the Ultra porosimeter. The porosity determined by this technique has the advantage of automatically accounting for bulk volume compressibility due to pore volume reduction at overburden stress.

Based upon the sample condition, the shape and dimensions for horizontal and vertical plug samples were deemed suitable for permeability testing, and all of them were selected for CMS TM-300 measurements. The direct pore volume, permeability to air, and Klinkenberg permeability of plug samples at ambient conditions were determined using Core Laboratories CMSTM-300. CMSTM-300 is an automated computer-controlled unsteady state pressure decay permeameter and porosimeter that measures pore volume, non-reactive liquid permeability (Klinkenberg), calculates an equivalent air permeability at a specified mean pressure, uses the Forchheimer Inertial Factor (Alpha and Beta), and uses the Klinkenberg slip factor at programmable, sequential confining stresses from 800 psig (minimum confining stress) to 10,000 psig on 1 and 1 1/2 inches in diameter.

A transient pressure fall-off technique is used by the instrument to evaluate permeability. Helium is poured into a tank whose capacity is precisely known. Helium is released into the environment through the hydrostatically stressed core sample. A calculation of the gas flow rate and pressure drop across the core sample at any given time is made possible by tracking the decaying tank pressure over time. This measurement's data are used to calculate the equivalent air permeability at a given mean pressure, the Klinkenberg slip factor, and the Forchheimer inertial factors (alpha and beta).

The statistical summary of the measured porosity (ø), horizontal permeability (K_h), and vertical permeability (K_v) of the studied samples (i.e., 369 experimental samples) is shown in Table 1.

Table 1. Statistical summary of the 369 experimental samples from carbonate formation.

Statistical Type	ø	K_h (mD)	K_v (mD)
Mean	0.11	4.802	5.1124
Minimum	0.005	0.12	0.09
Maximum	0.229	293	330
Count	369	369	369

4. Results and Discussion

In this section, we developed new correlations to predict vertical permeability for carbonate reservoirs as a function of horizontal permeability and porosity using a nonlinear regression approach. Firstly, we developed a new correlation for predicting vertical permeability for the whole data (369 samples; Table 1) as a function of horizontal permeability and porosity. The results indicate that the best form representing the relationship of vertical permeability with horizontal permeability and porosity is found to be as follows:

$$K_v = 0.339\frac{k_h^{1.204}}{\varnothing^{0.082}} \text{ for } 0.1 > (K_v/K_h) > 10 \text{ (369 samples)} \quad (9)$$

This new correlation is able to predict the vertical permeability with correlation coefficients (RSQ) of 0.853. Figure 1 shows the vertical permeability (measured and estimated from the developed correlation; Equation (9)) as a function of horizontal permeability and porosity. Figure 1 indicates that the new correlation estimates the vertical permeability with good accuracy.

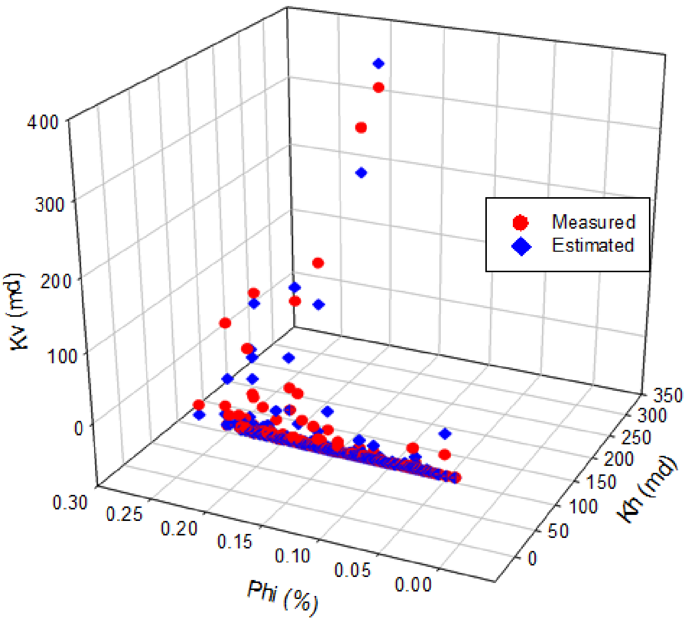

Figure 1. Comparison between the estimated (from Equation (9)) and measured vertical permeability vs. porosity and horizontal permeability using 369 experimental samples of the studied carbonate formation.

In order to increase the accuracy of the prediction vertical permeability, the used data (369 samples) were divided into four groups depending on the anisotropy (K_v/K_h) values, which are less than 0.1, 0.1–1, 1–10, and more than 10. Subsequently, a new correlation for predicting the vertical permeability of each data group as a function of the horizontal permeability and porosity has been developed. The following correlations were identified for each group:

$$K_v = -0.3738\left(\frac{K_h}{\varnothing}\right)^3 + 10.614\left(\frac{K_h}{\varnothing}\right)^2 - 53.374\left(\frac{K_h}{\varnothing}\right) + 77.72 \text{ for } (K_v/K_h) > 10 \quad (10)$$

$$K_v = 2.037\frac{k_h^{0.762}}{\varnothing^{0.487}} \text{ for } 1 < (K_v/K_h) < 10 \quad (11)$$

$$K_v = 0.818\left(K_h^{1.864}\right)\left(\varnothing^{2.503}\right) \text{ for } 0.1 < (K_v/K_h) < 1 \quad (12)$$

$$K_v = 0.193 + 0.001\left(\frac{K_h}{\varnothing}\right) \text{ for } (K_v/K_h) < 0.1 \quad (13)$$

The range of input and output variables that are used to develop the new correlations (Equations (10)–(13)) is summarized in Table 2. To check the accuracy of our established new correlations, the output data for prediction were compared with the experimental results. The correlation coefficient (RSQ) for the new correlations was 0.826 for group 1 data with $(K_v/K_h) > 10$ (Equation (10)), 0.963 for group 2 data with $1 < (K_v/K_h) < 10$ (Equation (11)), 0.947 for group 3 data with $0.1 < (K_v/K_h) < 1$ (Equation (12)), and 0.751 for group 4 data with $(K_v/K_h) < 0.1$ (Equation (13)). The statistical analysis above reveals high values of the correlation coefficient, indicating the high accuracy of our developed correlations (Equations (9)–(12)). Furthermore, Figures 2–5 cross-plot the experimentally measured vertical permeability versus those determined from new correlations (Equations (9)–(13)). The highly demonstrated agreements suggest that our proposed correlations are able to predict the vertical permeability for carbonate reservoirs as a function of horizontal permeability and porosity with excellent accuracy (Figures 2–5) and Table 3.

Table 2. Range data used to develop the new correlations (Equations (10)–(13)).

Statistical Type	Group 1 $(K_v/K_h) > 10$			Group 2 $1 < (K_v/K_h) < 10$			Group 3 $0.1 < (K_v/K_h) < 1$			Group 4 $(K_v/K_h) < 0.1$		
	ø	K_h	K_v	ø	K_h	K_v	ø	K_h	K_v	ø	K_h	K_v
Mean	0.112	0.5	12.0	0.12	7.24	11.35	0.105	2.616	1.407	0.103	13.22	0.382
Minimum	0.04	0.19	2.5	0.005	0.12	0.13	0.012	0.12	0.09	0.026	1.6	0.1
Maximum	0.14	3	31	0.229	293	330	0.202	123	108	0.211	70	1.8
Count	12	12	12	127	127	127	207	207	207	23	23	23

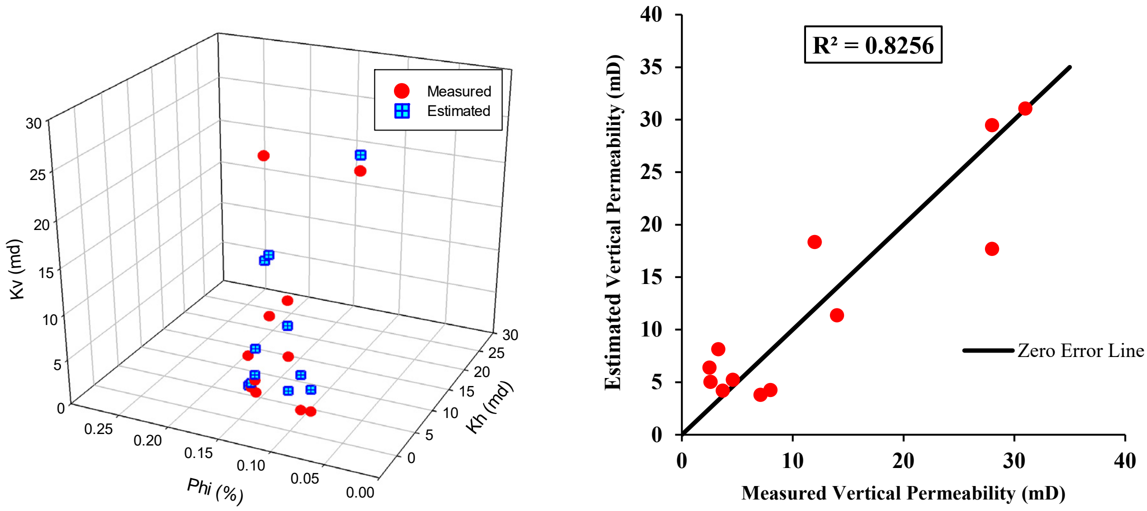

Figure 2. (**Left**): Three-dimensional (3D) scatter plot showing a comparison between the estimated (from Equation (10)) and measured vertical permeability vs. porosity and horizontal permeability for group 1 data: $(K_v/K_h) > 10$. (**Right**): Two-dimensional (2D) cross-plot of the measured and predicted vertical permeability from the newly developed correlation (Equation (10)).

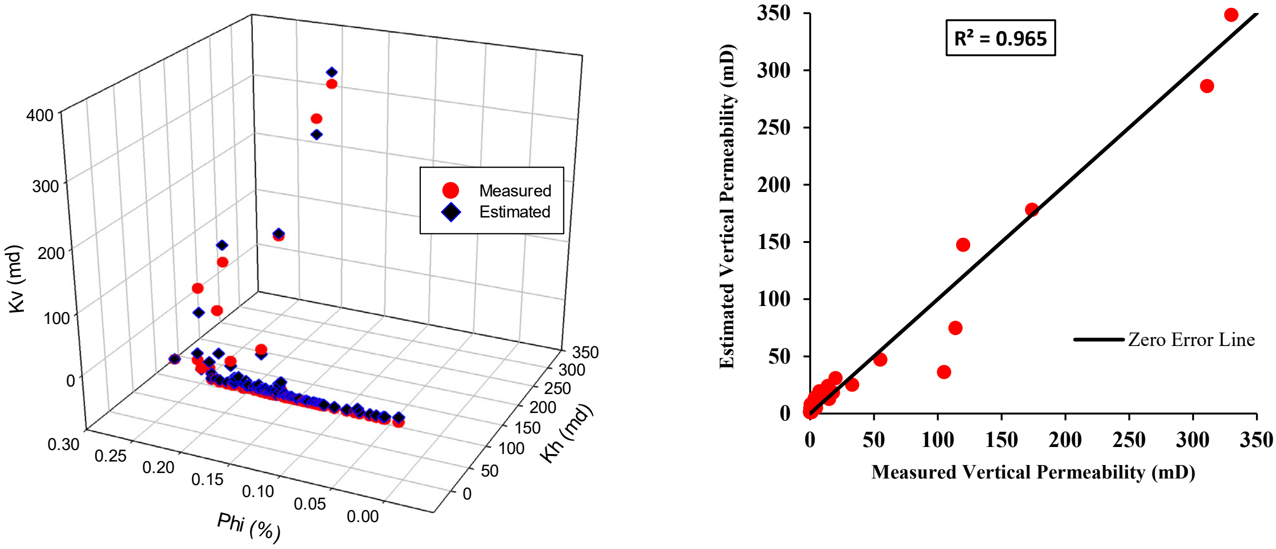

Figure 3. (**Left**): Three-dimensional (3D) scatter plot showing a comparison between the estimated (from Equation (11)) and measured vertical permeability vs. porosity and horizontal permeability for group 2 data: $1 < (K_v/K_h) < 10$. (**Right**): Two-dimensional (2D) cross-plot of the measured and predicted vertical permeability from the newly developed correlation (Equation (11)).

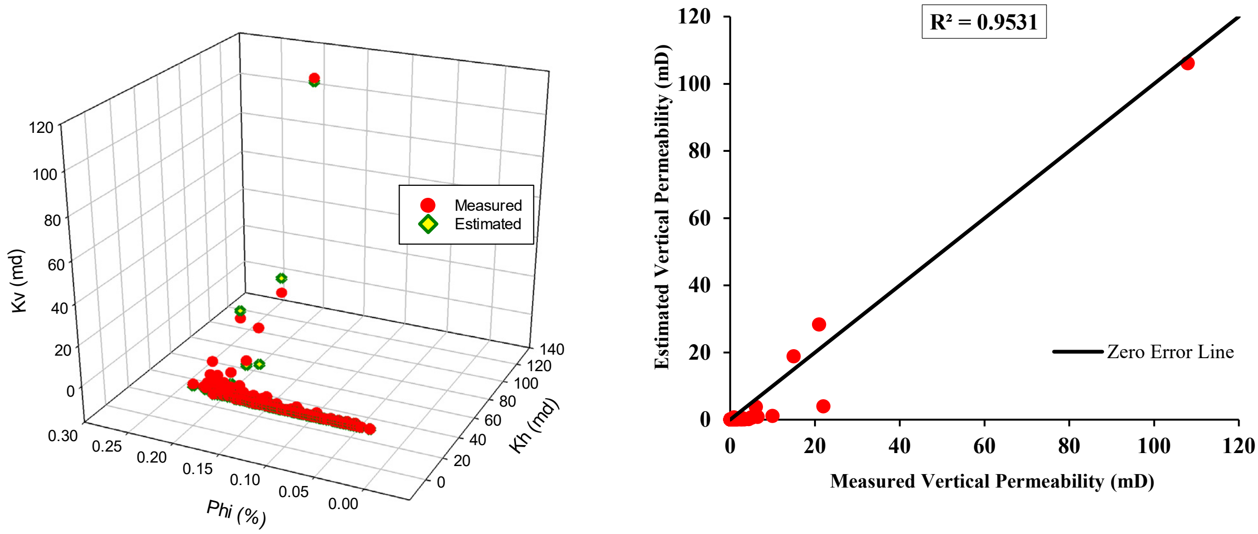

Figure 4. (**Left**): Three-dimensional (3D) scatter plot showing a comparison between the estimated (from Equation (12)) and measured vertical permeability vs. porosity and horizontal permeability for group 3 data: $0.1 < (K_v/K_h) < 1$. (**Right**): Two-dimensional (2D) cross-plot of the measured and predicted vertical permeability from the newly developed correlation (Equation (12)).

Table 3. Statistical accuracy of the developed correlations.

The New Developed Correlations	(K_v/K_h) Range	RSQ
Equation (9)	$0.1 > (K_v/K_h) > 10$	0.853
Equation (10)	$(K_v/K_h) > 10$	0.826
Equation (11)	$1 < (K_v/K_h) < 10$	0.963
Equation (12)	$0.1 < (K_v/K_h) < 1$	0.947
Equation (13)	$(K_v/K_h) < 0.1$	0.751

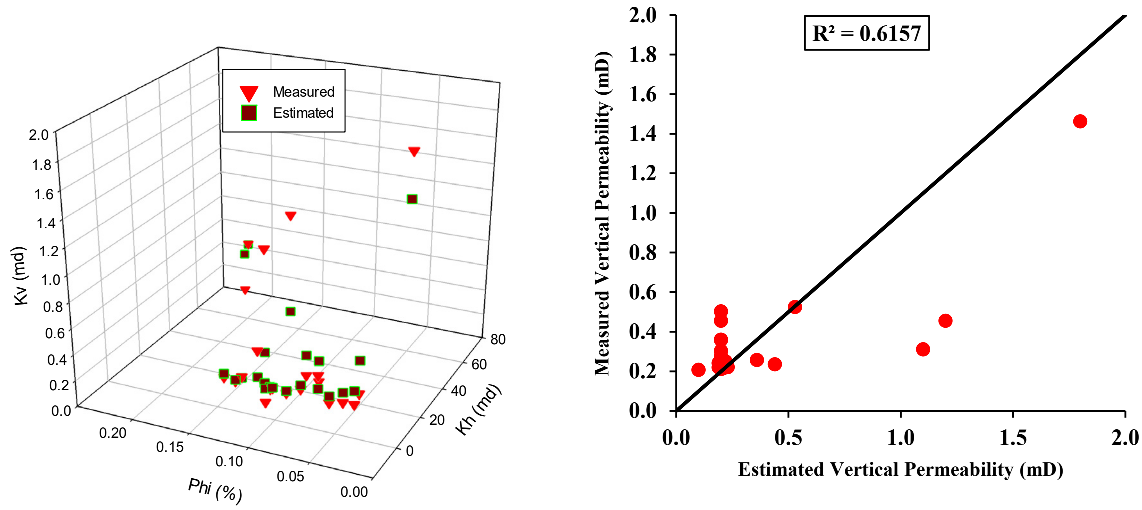

Figure 5. (**Left**): Three-dimensional (3D) scatter plot showing a comparison between the estimated (from Equation (13)) and measured vertical permeability vs. porosity and horizontal permeability for group 4 data: $(K_v/K_h) < 0.1$. (**Right**): Two-dimensional (2D) cross-plot of the measured and predicted vertical permeability from the newly developed correlation (Equation (13)).

5. Conclusions

Vertical permeability can be measured in the laboratory, but this process is time consuming. Although several correlations were presented to predict the vertical permeability of sandstone, predicting the vertical permeability of carbonate has not been investigated previously.

Thus, here, five new correlations for predicting the vertical permeability of carbonate reservoirs as a function of porosity and horizontal permeability have been developed. A total of 369 experimental measurements for the vertical permeability, porosity, and horizontal permeability of a selected carbonate reservoir have been used in this study. These data were separated into four groups depending on the ratio of vertical to horizontal permeability. The estimated vertical permeability of carbonate from the new correlation has been compared with the measured ones. The results indicate that the new correlations estimate vertical permeability with high accuracy. The new correlations predict the vertical permeability with very high correlation coefficients (R ranges from 0.751 to 0.963). Thus, we conclude that our new correlations can predict the vertical permeability of carbonates from porosity and horizontal permeability.

Author Contributions: Conceptualization, E.A.A.-K. and W.I.A.-R.; methodology, E.A.A.-K. and S.I.; software, R.H.A.; validation, W.I.A.-R.; formal analysis, E.A.A.-K. and W.I.A.-R.; investigation, E.A.A.-K. and R.H.A.; resources, W.I.A.-R.; data curation, W.I.A.-R.; writing—original draft preparation, R.H.A. and W.I.A.-R.; writing—review and editing S.I.; visualization, E.A.A.-K. and R.H.A. All authors have read and agreed to the published version of the manuscript.

Funding: This research received no external funding.

Data Availability Statement: The data presented in this study are available on request from the corresponding author.

Conflicts of Interest: The authors declare no conflict of interest.

References

1. Male, F.; Jensen, J.L.; Lake, L.W. Comparison of permeability predictions on cemented sandstones with physics-based and machine learning approaches. *J. Nat. Gas Sci. Eng.* **2020**, *77*, 103244. [CrossRef]
2. Sander, R.; Pan, Z.; Connell, L.D. Laboratory measurement of low permeability unconventional gas reservoir rocks: A review of experimental methods. *J. Nat. Gas Sci. Eng.* **2017**, *37*, 248–279. [CrossRef]

3. Basbug, B.; Karpyn, Z.T. Estimation of permeability from porosity, specific surface area, and irreducible water saturation using an artificial neural network. In Proceedings of the Latin American & Caribbean Petroleum Engineering Conference, Buenos Aires, Argentina, 15–18 April 2007.
4. Abdulraheem, A.; Sabakhy, E.; Ahmed, M.; Vantala, A.; Raharja, I.; Korvin, G. Estimation of permeability from wireline logs in a middle eastern carbonate reservoir using fuzzy logic. In Proceedings of the SPE Middle East Oil and Gas Show and Conference, Manama, Bahrain, 11–14 March 2007.
5. Huang, Z.; Shimeld, J.; Williamson, M.; Katsube, J. Permeability prediction with artificial neural network modeling in the Venture gas field, offshore eastern Canada. *Geophysics* **1996**, *61*, 422–436. [CrossRef]
6. Ngo, V.T.; Lu, V.D.; Nguyen, M.H.; Hoang, T.M.; Nguyen, H.M.; Le, V.M. A comparison of permeability prediction methods using core analysis data. In Proceedings of the SPE Reservoir Characterisation and Simulation Conference and Exhibition, Abu Dhabi, United Arab Emirates, 14–16 September 2015.
7. Al-Saddique, M.; Hamada, G.; Al-Awad, M.N. State of the art: Review of coring and core analysis technology. *J. King Saud Univ. Eng. Sci.* **2000**, *12*, 117–137. [CrossRef]
8. Tiab, D.; Donaldson, E.C. *Petrophysics: Theory and Practice of Measuring Reservoir Rock and Fluid Transport Properties*; Gulf Professional Publishing: Houston, TX, USA, 2015.
9. Mahdi, D.S.; Al-Khdheeawi, E.A.; Yuan, Y.; Zhang, Y.; Iglauer, S. Hydrogen underground storage efficiency in a heterogeneous sandstone reservoir. *Adv. Geo-Energy Res.* **2021**, *5*, 437–443. [CrossRef]
10. Fauziah, C.A.; Al-Khdheeawi, E.A.; Iglauer, S.; Barifcani, A. Effect of clay minerals heterogeneity on wettability measurements: Implications for CO_2 storage. In Proceedings of the Offshore Technology Conference Asia (p. D012S001R101), Kuala Lumpur, Malaysia, 2–6 November 2020.
11. Al-Khdheeawi, E.A.; Vialle, S.; Barifcani, A.; Sarmadivaleh, M.; Iglauer, S. The effect of $WACO_2$ ratio on CO_2 geo-sequestration efficiency in homogeneous reservoirs. *Energy Procedia* **2018**, *154*, 100–105. [CrossRef]
12. Al-Khdheeawi, E.A.; Mahdi, D.S.; Yuan, Y.; Iglauer, S. Influence of Clay Content on CO_2-Rock Interaction and Mineral-Trapping Capacity of Sandstone Reservoirs. *Energies* **2023**, *16*, 3489. [CrossRef]
13. Al-Khdheeawi, E.A.; Mahdi, D.S.; Hasan, M.M. Reservoir scale CO_2-water-rock interactions and geochemical evolution of sandstone reservoirs due to CO_2 geo-storage process. *AIP Conf. Proc.* **2022**, *2443*, 030007.
14. Clark, N.J. *Elements of Petroleum Reservoirs*; Society of Petroleum Engineers: Richardson, TX, USA, 1969.
15. Babadagli, T.; Al-Salmi, S. A review of permeability-prediction methods for carbonate reservoirs using well-log data. *SPE Reserv. Eval. Eng.* **2004**, *7*, 75–88. [CrossRef]
16. Kamal, M.M.; Morsy, S.; Suleen, F.; Pan, Y.; Dastan, A.; Stuart, M.R.; Mire, E.; Zakariya, Z. Determination of in-situ reservoir absolute permeability under multiphase-flow conditions using transient well testing. *SPE Reserv. Eval. Eng.* **2019**, *22*, 336–350. [CrossRef]
17. Zakirov, T.; Galeev, A. Absolute permeability calculations in micro-computed tomography models of sandstones by Navier-Stokes and lattice Boltzmann equations. *Int. J. Heat Mass Transf.* **2019**, *129*, 415–426. [CrossRef]
18. Yao, C.; Holditch, S. Estimating permeability profiles using core and log data. In Proceedings of the SPE Eastern Regional Meeting, Pittsburgh, PA, USA, 2–4 November 1993.
19. Qin, Z.; Wu, D.; Luo, S.; Ma, X.; Huang, K.; Tian, F.; Xiao, K.; Chen, X.; Hou, M.; Pan, H. A novel method to obtain permeability in a dual-pore system using geophysical logs: A case study of an Upper Triassic Formation, Southwest Ordos Basin, China. *Nat. Resour. Res.* **2020**, *29*, 2619–2634. [CrossRef]
20. Armstrong, O.P. Permeability Correlations for Carbonate and Other Rocks. In Proceedings of the 2003 Seattle Annual Meeting, Seattle, WA, USA, 2–5 November 2003.
21. Gholinezhad, S.; Masihi, M. A physical-based model of permeability/porosity relationship for the rock data of Iran southern carbonate reservoirs. *Iran. J. Oil Gas Sci. Technol.* **2012**, *1*, 25–36.
22. Kozeny, J. Uber kapillare Leitung des Wassers im Boden-Aufstieg, Versickerung und Anwendung auf die Bewasserung, Sitzungsberichte der Akademie der Wissenschaften Wien. *Math. Naturwissenschaftliche Abt.* **1927**, *136*, 271–306.
23. Carman, C. Fluid flow through granular beds. *Chem. Eng. Res. Des.* **1997**, *75*, S32–S48. [CrossRef]
24. Chapuis, R.P.; Aubertin, M. On the use of the Kozeny Carman equation to predict the hydraulic conductivity of soils. *Can. Geotech. J.* **2003**, *40*, 616–628. [CrossRef]
25. Amaefule, J.O.; Altunbay, M.; Tiab, D.; Kersey, D.G.; Keelan, D.K. Enhanced reservoir description: Using core and log data to identify hydraulic (flow) units and predict permeability in uncored intervals/wells. In Proceedings of the SPE Annual Technical Conference and Exhibition, Houston, TX, USA, 3–6 October 1993.
26. Zahaf, K.; Tiab, D. Vertical permeability from in situ horizontal measurements in shaly-sand reservoirs. *J. Can. Pet. Technol.* **2002**, *41*, 43–50. [CrossRef]
27. Aqrawi, A.A.M.; Thehni, G.A.; Sherwani, G.H.; Kareem, B.M.A. Mid-Cretaceous rudist-bearing carbonates of the Mishrif Formation: An important reservoir sequence in the Mesopotamian Basin, Iraq. *J. Pet. Geol.* **1998**, *21*, 57–82. [CrossRef]
28. Mahdi, A.Q.; Abdel-Fattah, M.I.; Radwan, A.E.; Hamdan, H.A. An integrated geochemical analysis, basin modeling, and palynofacies analysis for characterizing mixed organic-rich carbonate and shale rocks in Mesopotamian Basin, Iraq: Insights for multisource rocks evaluation. *J. Pet. Sci. Eng.* **2022**, *216*. [CrossRef]

29. Mahdi, T.A.; Aqrawi, A.A.; Horbury, A.D.; Sherwani, G.H. Sedimentological characterization of the mid-Cretaceous Mishrif reservoir in southern Mesopotamian Basin, Iraq. *GeoArabia* **2013**, *18*, 139–174. [CrossRef]
30. Sadooni, F.N. The nature and origin of Upper Cretaceous basin-margin rudist buildups of the Mesopotamian Basin, southern Iraq, with consideration of possible hydrocarbon stratigraphic entrapment. *Cretac. Res.* **2005**, *26*, 213–224. [CrossRef]
31. Liu, H.; Shi, K.; Liu, B.; Song, X.; Guo, R.; Wang, G.; Wang, H. Microfacies and reservoir quality of the Middle Cretaceous Rumaila Formation in the AD oilfield, central Mesopotamian Basin, southern Iraq. *J. Asian Earth Sci.* **2021**, *213*. [CrossRef]